Am J Cancer Res 2025;15(8):3693-3711
www.ajcr.us /ISSN:2156-6976/ajcr0164900

Original Article

Aurora-A inhibits hepatocellular carcinoma cell ferroptosis to mediate immune escape by disrupting phosphatidylethanolamine biosynthesis

Lei Fan[1,2*], Yiqian Liu[3*], Yucheng Cai[4], Xinnan Sun[4], Jiaxuan Li[4], Yiyang Xu[4], Changchun Sun[5], Shiyun Cui[3,6]

[1]Department of General Surgery, Affiliated Hospital of Integrated Traditional Chinese and Western Medicine, Nanjing University of Chinese Medicine, Nanjing, Jiangsu, P. R. China; [2]Department of General Surgery, Jiangsu Province Academy of Traditional Chinese Medicine, Nanjing, Jiangsu, P. R. China; [3]Department of Oncology, The First Affiliated Hospital of Nanjing Medical University, Nanjing, Jiangsu, P. R. China; [4]Nanjing Medical University, Nanjing, Jiangsu, P. R. China; [5]Department of Oncology, Jingjiang People's Hospital Affiliated to Yangzhou University, Jingjiang, Jiangsu, P. R. China; [6]Department of Oncology, Chongqing Hospital of Jiangsu Province Hospital (The People's Hospital of Qijiang District), Chongqing, P. R. China. [*]Equal contributors.

Received March 29, 2025; Accepted August 20, 2025; Epub August 25, 2025; Published August 30, 2025

Abstract: This study aims to explore Aurora-A's role in regulating immune escape of hepatocellular carcinoma (HCC). We performed non-targeted metabolomics analysis and analyzed the impact of Aurora-A inhibitor Alisertib on anti-PD-1 therapy efficacy on xenograft tumors and co-culture models of $CD8^+$ T cells and HCC cells. We determined reactive oxygen species (ROS) and malondialdehyde (MDA) production in HCC cells to evaluate lipid peroxidation. Confocal images of endoplasmic reticulum (ER) and mitochondria in HCC cells were taken to assess the role of Aurora-A and dynamin-related protein 1 (Drp-1) on mitochondria-associated endoplasmic reticulum membranes (MAMs) formation. The results showed that Aurora-A was upregulated in HCC cells and its knockdown significantly augmented phosphatidylethanolamine (PE) production while having no effect on phosphatidylserine decarboxylase (PSD). Further, Aurora-A inhibitor Alisertib enhanced the sensibility of HCC cells to anti-PD-1 therapy and $CD45^+CD8^+$ T cell infiltration in HCC tumors. To conclude, our work revealed that Aurora-A dysregulated PS/PE metabolism via facilitating Drp1-Ser616 phosphorylation to disrupt MAMs formation, resulting in suppressed ferroptosis in HCC cells to reduce their sensitivity to anti-PD-1.

Keywords: HCC, Aurora-A, ferroptosis, MAMs formation, immune escape

Introduction

Globally, hepatocellular carcinoma (HCC) is one of the most frequent cancer types and the third leading cause of cancer-related death [1]. Generally, surgical resection is the first choice for HCC patients, but most of them are not suitable for surgery. Non-surgical therapies, including radiotherapy, chemotherapy, immunotherapy, transarterial chemoembolization, local ablation therapy, have been applied to relieve patients' symptoms, but the overall prognosis is still not satisfactory [2]. Programmed cell death protein 1 (PD-1) is an immune checkpoint molecule that is highly related to tumor immune evasion [3]. Its inhibitors have been approved for HCC treatment [4]. However, not all HCC cases are sensitive to anti-PD-1 therapy. Hence, new and more biomarkers remain to be identified in HCC.

Aurora-A is a serine/threonine protein kinase belonging to the Aurora kinase family [5]. Aurora-A, also called STK15, has been proven to be highly expressed in HCC and be relevant to the unfavorable prognosis of HCC patients [6]. Importantly, previous reports have revealed that Aurora-A plays a pivotal role in regulating HCC cell functions and cell resistance to different therapies [7-9]. Besides, Aurora-A inhibitors have also been reported to be effective in enhancing chemosensitivities of HCC cells [10, 11]. Nevertheless, the influences of Aurora-A and its inhibitors on immune therapies like anti-PD-1 remain unknown.

https://doi.org/10.62347/JTQO8098

Metabolic reprogramming is a hallmark of tumors. The metabolic characteristics of tumors take changes during cancer development [12]. Overlapping metabolic reprogramming of tumor and immune cells is thought to be a determinant of anti-tumor immune response in malignancies [13]. Recently, Aurora-A has been indicated to regulate glycolysis in several different types of cancer cells and phospholipid remodeling in glioblastoma [14, 15]. Based on these reports, we hypothesized that Aurora-A and its inhibitors might affect HCC cell metabolism to modulate immune therapy efficacy.

In this study, we aim to testify above hypothesis and investigate the underlying mechanism through which Aurora-A regulates HCC cell metabolism. According to investigations, Aurora-A dysregulates phosphatidylserine/phosphatidylethanolamine (PS/PE) metabolism through promoting the phosphorylation of dynamin-related protein 1 (Drp1) at Ser616 to impede mitochondria-associated endoplasmic reticulum membranes (MAMs) formation, finally leading to hindered ferroptosis in HCC cells to reduce sensitivity of anti-PD-1. The findings suggest Aurora-A inhibitors as a new possible target for HCC treatment.

Materials and methods

Cell culture

The healthy liver-derived human cell line (THLE-2) and HCC cell lines (LM3, Huh7, HepG2, and Hep3B) were purchased from the American Type Culture Collection (ATCC. Manassas, VA, USA). Cells were all grown in DMEM (Invitrogen Life Technologies, Carlsbad, CA, USA) containing 10% fetal bovine serum (FBS, Invitrogen) and 1% penicillin-streptomycin (Invitrogen). The cell culture plates were placed in a humidified incubator with 5% CO_2 at 37°C. The media were changed every 2-3 days.

Cell transfection

For AURKA knockdown, cells were transfected with three different siRNAs targeting AURKA (si-AURKA#1/2/3) or si-NC (negative control) using Lipofectamine™ 3000 Reagent (Lipo3000, Invitrogen, California, USA). pcDNA3.1 vectors (Invitrogen) were applied to overexpress AURKA in indicated HCC cells. After transfection for 48 h, the transfection efficiencies were evaluated via RT-qPCR.

RNA isolation and reverse transcription-real time PCR (RT-qPCR)

Total RNA was isolated using Trizol reagent (TaKaLa, Dalian, China) and then reversely transcribed into cDNA via the Reverse Transcription Kit (Takara, Dalian, China). Real-time PCR analysis was conducted with SYBR Premix Ex Taq (Takara, Dalian China). GAPDH was used as the endogenous control. The RT-qPCR was performed on an ABI 7500 Real-Time PCR System (Applied Biosystems, Foster City, CA). Relative gene expression was evaluated with the $2^{-\Delta\Delta Ct}$ method.

Non-targeted metabolite analysis

After samples were extracted according to a published protocol by Shanghai Lu-Ming Biotech Co. Ltd. (Shanghai, China, 2021), non-targeted metabolite analysis was implemented via OE Biotech (Shanghai, China). To analyze the metabolic profiling, a Dionex Ultimate 3000 RS UHPLC system fitted with a Q-Exactive quadrupole-Orbitrap mass spectrometer and equipped with heated electrospray ionization (ESI) source (Thermo Fisher Scientific, Waltham, MA, USA) was applied. The acquired LC-MS raw datasets were analyzed through progenesis QI software (Waters Corporation, Milford, USA).

Measurement of PS, PE and phosphatidylserine decarboxylase (PSD)

The contents of PS, PE, and PSD were determined as previously described [16].

Western blotting

Protein lysates were obtained via RIPA buffer containing proteinase inhibitors (R0278, Sigma-Aldrich St. Louis, MO, USA). Proteins were isolated using 10% sodium dodecyl sulfate-polyacrylamide gel electrophoresis (SDS-PAGE) and then transformed into nitrocellulose (NC) membrane. Next, the membranes were blocked in 5% non-fat milk, followed by incubation with primary antibodies, including anti-NCOA4 (1:1000 dilution, Cambridge, ab314553, Abcam, CA, USA), anti-ACSL4 (1:10000 dilution, ab155282, Abcam), anti-GLS2 (1:1000 dilution, ab308304, Abcam), anti-Aurora-A (1:1000 dilution, ab61114, Abcam), anti-Drp1 (1:1000 dilution, ab184247, Abcam), anti-DRP1-Ser616 (1:1000 dilution, ab314755, Abcam), anti-Drp1-

Ser637 (1:1000 dilution, ab193216, Abcam), and the loading control anti-β-actin (1:5000 dilution, ab179467, Abcam) at 4°C overnight. After washing, the membranes were treated with the HRP-conjugated secondary antibody (1:2000 dilution, ab288151, Abcam) for 2 hours. The protein bands were visualized through the ECL detection system (32134, Pierce Biotechnology, Rockford, IL, USA) and then quantitated via Quantity One software (Bio-Rad, Hercules, CA, USA).

In vivo experiments

Male C57B/L6 mice (8 weeks, 18±2 g) were brought from The Jackson Laboratory. All mice were reared under a specific pathogen-free environment with 50-60% humidity and a temperature of 22°C. All mice were exposed to 12-hour light/dark cycle and had free access to food and water. All mice were allowed 3-7 days for adaptation after arrival before experiments. The xenograft model was established via subcutaneous injection of indicated HCC cells into the left backs of mice. Tumor volumes were measured every 3 days based on the formula: V = 0.5 × D × d2 (V: volume; D: the longitudinal diameter; d: the latitudinal diameter). After the tumor volume exceeds 50 mm^3, mice were treated with Aurora-A inhibitor Alisertib or anti-PD-1 which is described in **Figure 2A**. Four weeks later, the tumors were obtained for subsequent analyses. Humane endpoints were strictly enforced when tumor-bearing mice exhibit either ≥ 20% body weight loss or inability to access food/water independently, requiring prompt euthanasia. To humanely euthanize C57BL/6 mice, CO_2 inhalation was used at a controlled flow rate of 28% chamber volume per minute, ensuring minimal distress and rapid unconsciousness.

Flow cytometry analysis of T cells

The live T cells were selected by staining with Fixable Viability Dye eFluor 450 (eBioscience) for 15 mins at 4°C and then incubated with primary antibodies against CD45 and CD8 (BioLegend). The stained T cells were captured by the BD FACSCanto II Flow Cytometer using BD FACSDiva software (BD Biosciences), and the generated data were processed with FlowJo software.

Immunohistochemistry (IHC) assay

The Ki67 staining in xenograft tumors was assessed via IHC. In brief, tumors after being fixed by formalin and embedded via paraffin were cut into sections. Then, the sections were treated with primary Ki67 antibodies for half an hour, followed by incubation with secondary antibody (DakoCytomation, Denmark) for 30 min. After being counterstained with hematoxylin, sections were processed by 3, 30-diaminobenzidine chromogen to visualize the signals.

Measurement of reactive oxygen species (ROS), malondialdehyde (MDA), glutathione (GSH) and iron contents

The lysates from HCC cells and xenograft tumors were attained by RIPA Lysis Buffer (Beyotime, China). Flow cytometry was applied for ROS analysis. MDA content was tested via the Lipid Peroxidation MDA Assay Kit (Beyotime, China). GSH level was determined with The Glutathione Assay Kit (Cayman Chemical). The iron contents in the lysates of xenograft tumors were estimated by using a Tissue Iron Assay Kit (Nanjing Jincheng, China).

Confocal fluorescence microscopy

Confocal fluorescence microscopy was used to measure the co-localization of ER and mitochondria as previously described [17]. Besides, the co-localization of Drp1 and mitochondria was also observed by confocal fluorescence microscopy, with the mitochondria stained by MitoTracker Red CMXRos (Beyotime Biotechnology) and Drp1 recognized by GFP-labeled specific antibodies. Also, the co-localization of PE and CD8 in T cells was observed via confocal fluorescence microscopy. In this experiment, PE-labeled by duramycin-LC-biotin (Molecular Targeting Technologies) and CD8 antibodies were applied. The nuclei were stained using DAPI.

Co-culture system of HCC cells and T cells

The transwell inserts were used for the co-culture model. Before co-culture, LM3 cells were treated with Alisertib or DMSO for 48 h. The media were replaced, together with a transwell (0.4 μm) inserted into a 6-well plate to create two spaces. In the co-culture model, LM3 cells were cultured in a 6-well plate while $CD8^+$ T

cells were grown on the surface of the transwell insert.

Statistical analysis

Data obtained from independent experiments repeated at least three times were expressed as mean ± SD. Differences between two groups were assessed via the student's t-test, whereas those among more than two groups were evaluated by using one-way ANOVA with Tukey post-hoc test. The statistical analyses were conducted by using SPSS v17.0 software. $P < 0.05$ indicated that the difference was statistically significant.

Results

Aurora-A modulates PS/PE metabolism in HCC cells

We first tested the expression of AURKA gene encoding Aurora kinase A and found that it was highly expressed in four HCC cells (HepG2, LM3, Huh7, and Hep3B) when compared to the healthy liver-derived human cell line THLE-2 (**Figure 1A**). Next, we separately knocked down and overexpressed the AURKA expression to further analyze its function in HCC (**Figure 1B**). Since Aurora-A has been revealed to be related to metabolic reprogramming-modulated cancer development [14], we analyzed its impact on HCC metabolism. Hence, we performed non-targeted metabolomics analysis after knocking down AURKA in LM3 cells. The results indicated that 54 metabolites were significantly up-regulated and 4 metabolites were down-regulated after AURKA knockdown, among which the most evidently up-regulated metabolite was PE (Figure S1). The KEGG pathway enrichment results uncovered that repressing Aurora-A expression had the significant influence on the glycerol phospholipid metabolic pathway (Figure S2). Importantly, knockdown of Aurora-A induced the most evident changes in the PE metabolite of this pathway (Figure S3). Based on these data, we further explored the impact of Aurora-A on PE metabolism in HCC cells. As expected, PE levels in HCC cells were enhanced after AURKA knockdown, while reduced by AURKA overexpression (**Figure 1C**, **1D**). PE is transformed from PS, and its synthesis is exclusively mediated by PSD (**Figure 1E**). Moreover, PS levels were increased in AURKA-downregulated HCC cells (**Figure 1F**). However, no changes were observed in PSD levels after AURKA knockdown (**Figure 1G**). In conclusion, Aurora-A prevents PE production in HCC cells by modulating PS/PE metabolism.

Aurora-A inhibitors promote ferroptosis to reinforce the efficacy of anti-PD-1 therapy for HCC

It has been reported that PE is one of the responsible factors for ferroptosis [18], which is highly related to cancer immunotherapy [19]. Besides, Aurora-A has been unveiled as a ferroptosis modulator in cancer [20]. Hence, we investigated that whether Aurora-A could affect ferroptosis, regulate HCC development and immune therapy by influencing PE metabolism. At first, we analyzed the impact of Aurora-A inhibitor Alisertib on xenograft HCC tumors treated with or without anti-PD-1 therapy. The details of treatments on xenograft tumors were shown in **Figure 2A**. Data showed that tumors were distinctly lessened after treatment with Alisertib or anti-PD-1 alone, but further suppressed when both Alisertib and anti-PD-1 were given (**Figure 2B-D**). Besides, flow cytometry analysis revealed that compared to the control group, the accumulation of $CD45^+CD8^+$ T cells was enhanced in the groups treated with Alisertib or anti-PD-1, and this trend was more significant in the group treated with both Alisertib and anti-PD-1 (**Figure 2E**). Meanwhile, IHC data indicated that the positivity of Ki67 was lower in the groups treated with Alisertib or anti-PD-1 than that in control group, and it was further reduced in the group treated with both Alisertib and anti-PD-1 (**Figure 2F**). These findings suggested that Aurora-A inhibition suppressed HCC tumor development and enhanced the efficacy of immune therapy. Next, we tested the changes in ferroptosis-related factors and PE content in these groups of tumors. It showed that Alisertib led to the augmentation of the iron content and the reduction of the GSH level in mice treated with or without anti-PD-1 compared with control or anti-PD-1 group (**Figure 2G**, **2H**). Additionally, the expression levels of AURKA and ferroptosis-related genes, including nuclear receptor coactivator 4 (NCOA4), acyl-CoA synthetase long-chain family member 4 (ACSL4), and glutaminase-2 (GLS2), were detected in four groups of tumor samples. As shown in **Figure 2I**, **2J**, the mRNA and protein levels of AURKA were decreased in tumor tissues of mice treated with Alisertib compared to control group. Similarly, both levels of AURKA in

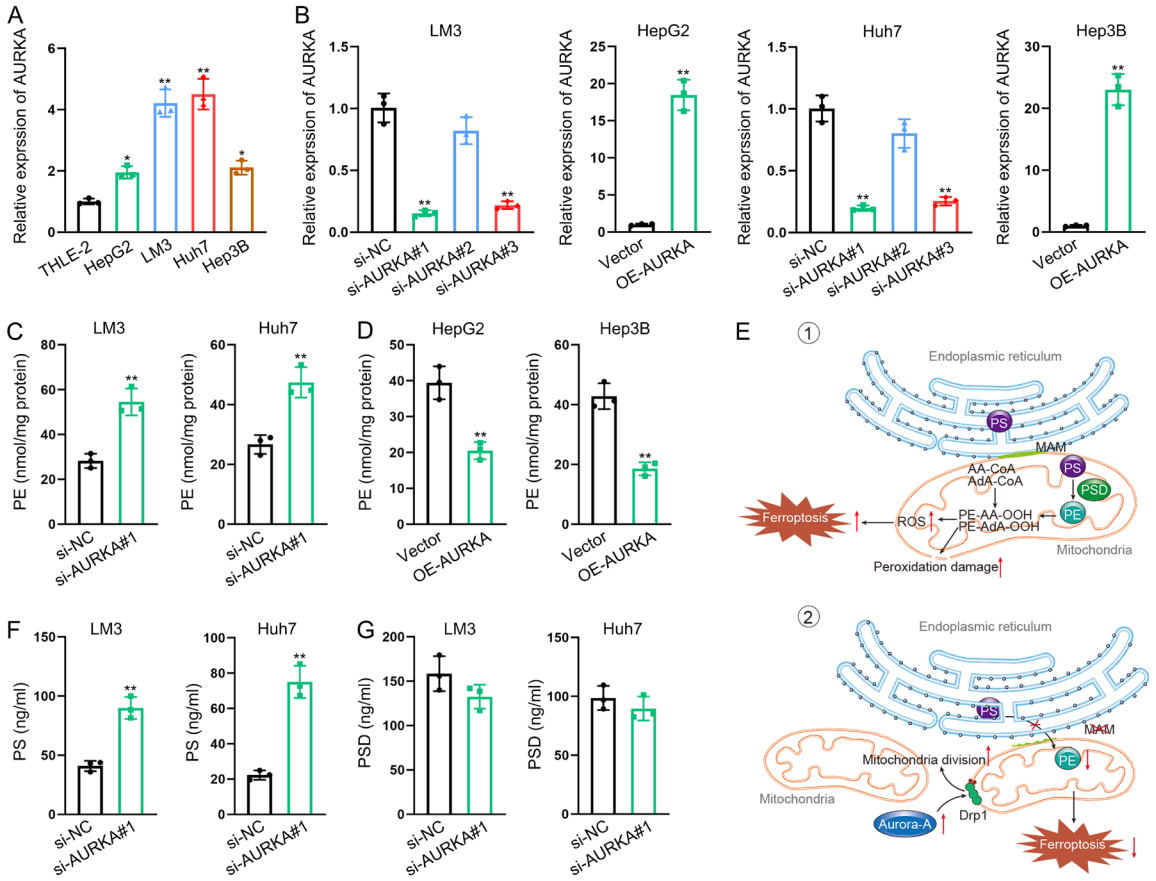

Figure 1. AURKA is overexpressed in HCC cells and suppresses PE production. A. AURKA mRNA expression in four HCC cells and the healthy THLE-2 cells were measured by RT-qPCR. B. The knockdown and overexpression efficiencies of AURKA in HCC cells was analyzed by RT-qPCR. C, D. PE contents were estimated in HCC cells under AURKA knockdown or overexpression. E. The mechanistic graph of PE biosynthesis pathway. F, G. The changes in PS and PSD contents were evaluated in HCC cells after AURKA knockdown. $^{*}P < 0.05$, $^{**}P < 0.01$.

mice treated with both Alisertib and anti-PD-1 were significantly lower than that in mice treated with anti-PD-1 alone. However, the mRNA and protein levels of three ferroptosis-related genes in four groups of mice showed a completely opposite trend compared to AURKA (**Figure 2I**, **2J**). Moreover, Alisertib treatment could increase PE content in mice treated with or without anti-PD-1 (**Figure 2K**). To sum up, inhibiting Aurora-A strengthens ferroptosis to improve the efficacy of immune therapy for HCC.

Aurora-A suppresses ferroptosis in HCC cells

Next, we evaluated the effects of Aurora-A on the ferroptosis of HCC cells. RT-qPCR and western blotting results indicated that both mRNA and protein levels of NCOA4, ACSL4, and GLS2 were markedly upregulated by the knockdown of AURKA, whereas they were all downregulated upon AURKA overexpression (**Figure 3A**, **3B**). Meanwhile, we observed the changes of ROS and MDA production in HCC cells to evaluate lipid peroxidation, a feature of ferroptosis. The data showed that AURKA knockdown led to an increase in ROS, while AURKA overexpression resulted in a decrease in ROS (**Figure 3C**). Similarly, MDA content was augmented by AURKA knockdown, while it was lessened after AURKA overexpression (**Figure 3D**). In summary, Aurora-A acts as a ferroptosis inhibitor in HCC cells.

Aurora-A inhibitors boost PE production to promote T cell activation

The above data indicate that Aurora-A prevents PE production to inhibit ferroptosis, and Aurora-A inhibitor strengthens ferroptosis to improve the efficacy of immune therapy for HCC. Here, we continued to explore whether

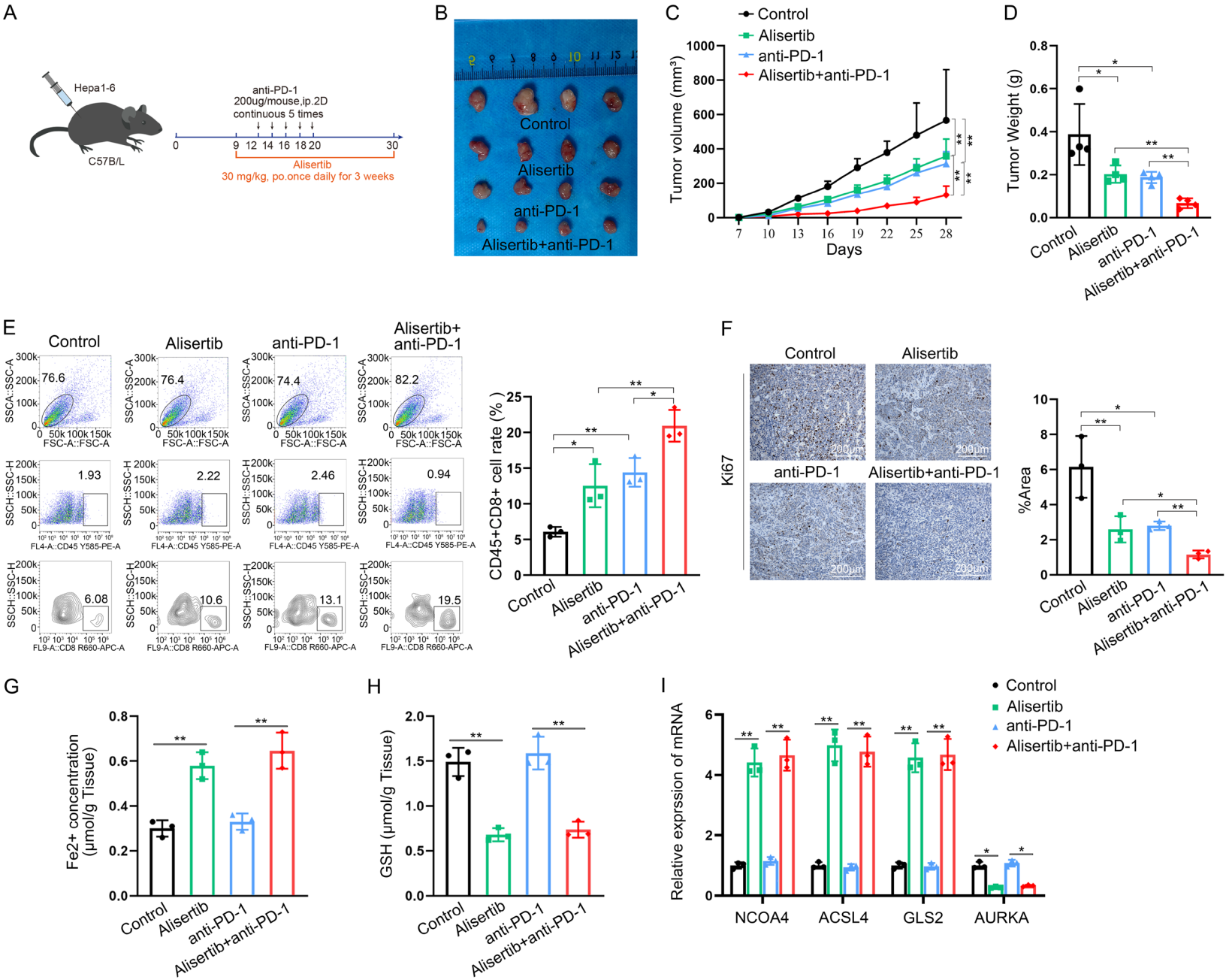
A
Hepa1-6
C57B/L
anti-PD-1
200ug/mouse,ip.2D
continuous 5 times
0
9 12 14 16 18 20
30
Alisertib
30 mg/kg, po.once daily for 3 weeks
B
Control
Alisertib
anti-PD-1
Alisertib+anti-PD-1
C
Control
Alisertib
anti-PD-1
Alisertib+anti-PD-1
Tumor volume (mm³)
Days
D
Tumor Weight (g)
Control
Alisertib
anti-PD-1
Alisertib+anti-PD-1
E
Control
Alisertib
anti-PD-1
Alisertib+ anti-PD-1
SSCA::SSC-A
FSC-A::FSC-A
SSCH::SSC-H
FL4-A::CD45 Y585-PE-A
FL9-A::CD8 R660-APC-A
76.6
76.4
74.4
82.2
1.93
2.22
2.46
0.94
6.08
10.6
13.1
19.5
CD45+CD8+ cell rate (%)
F
Control
Alisertib
anti-PD-1
Alisertib+anti-PD-1
Ki67
200μm
%Area
G
Fe2+ concentration (μmol/g Tissue)
H
GSH (μmol/g Tissue)
I
Relative exprssion of mRNA
NCOA4
ACSL4
GLS2
AURKA

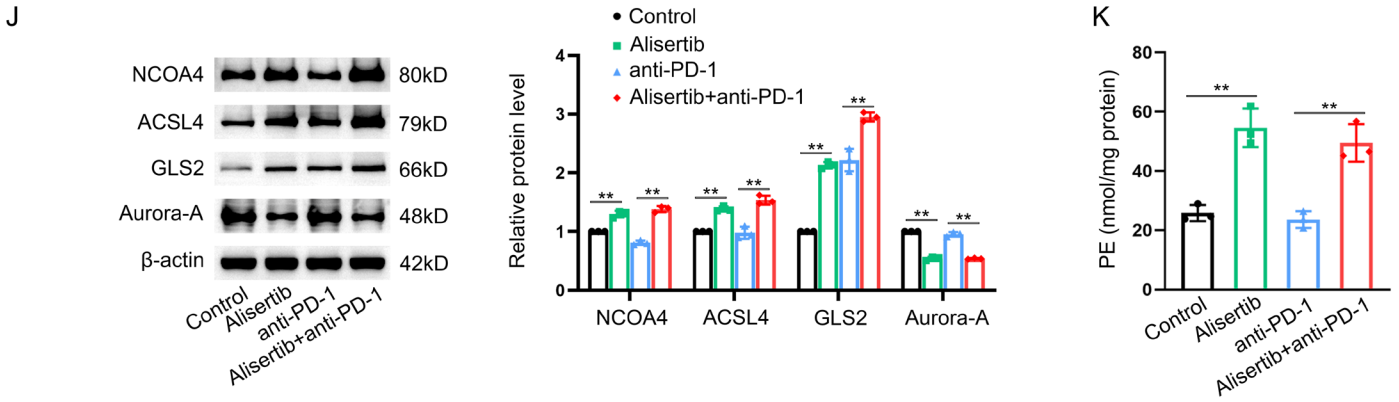

Figure 2. Combination treatment of Alisertib elevates anti-PD-1 therapy efficacy for HCC tumors. A. The injection project of mice loading xenograft HCC tumors. B. Images of tumors isolated from indicated groups of mice. C, D. Tumor growth curves and tumor weights were presented. E. Changes in the infiltration of $CD45^{+}CD8^{+}$ T cells in xenograft tumors were analyzed by flow cytometry. F. IHC analyses of Ki67 staining in xenograft tumors. Scale bar = 200 μm. G, H. The iron and GSH contents in the lysates of each group of tumors were evaluated. I, J. The expression levels of ferroptosis-related genes (including NCOA4, ACSL4 and GLS2) and AURKA were detected in four groups of tumors via RT-qPCR and western blotting. K. PE concentrations in the lysates of four groups of xenograft tumors were measured. $^{*}P < 0.05$, $^{**}P < 0.01$.

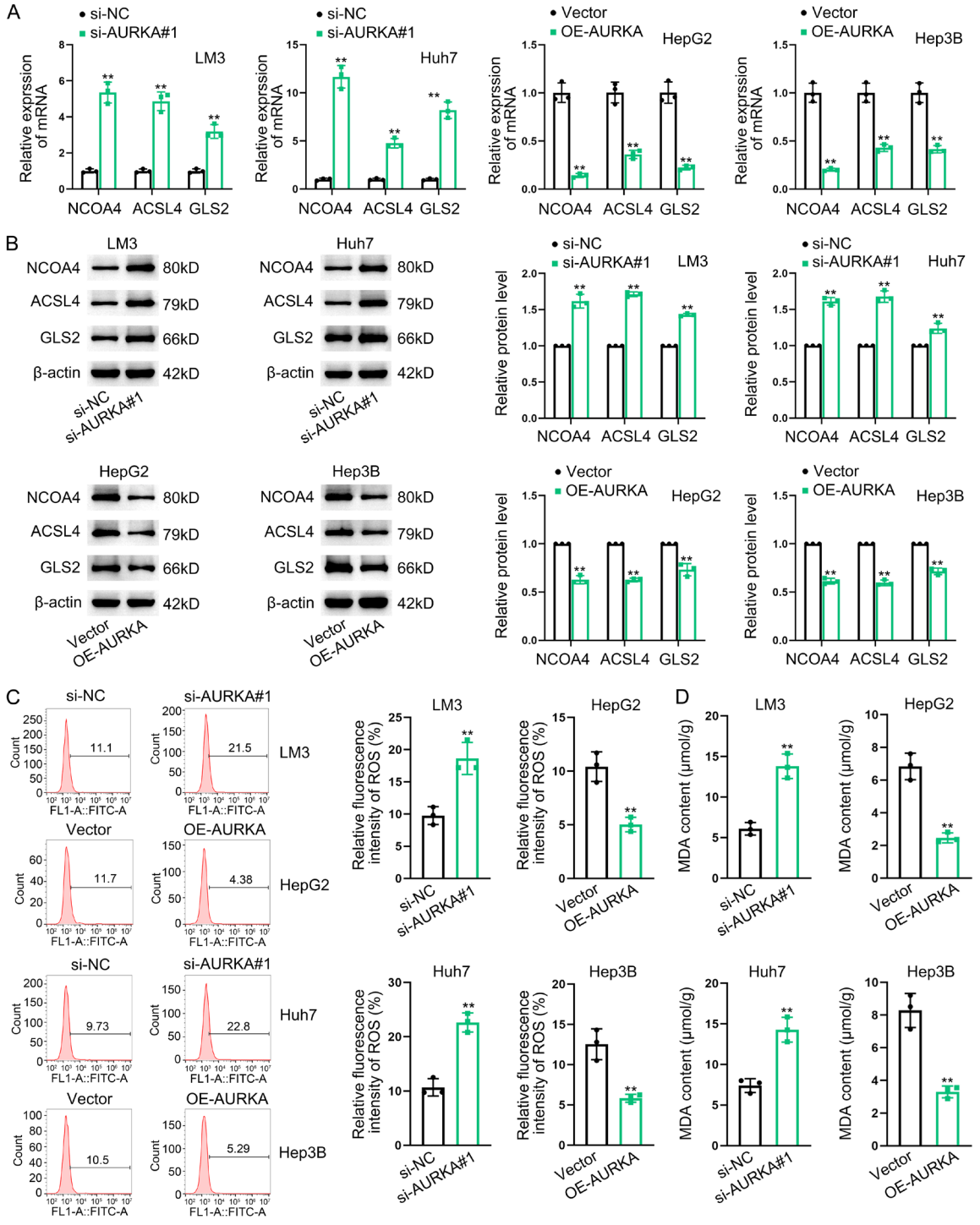

Figure 3. AURKA negatively regulates ferroptosis in HCC cells. A, B. The expression of NCOA4, ACSL4 and GLS2 in HCC cells with AURKA knockdown or overexpression was examined by RT-qPCR and western blotting. C. The effect of AURKA knockdown or overexpression on the ROS level in HCC cells was evaluated. D. The changes in MDA contents in HCC cells with AURKA knockdown or overexpression were tested. $^{**}P < 0.01$.

Aurora-A inhibitors affected T cell activation and immune therapy through regulating PE. As expected, the addition of Aurora-A inhibitor Alisertib increased PE content in HCC cells (**Figure 4A**). Next, the co-culture model of $CD8^+$ T cells and LM3 cells treated with or without Alisertib was established (**Figure 4B**). It manifested that $CD8^+$ T cells co-cultured with

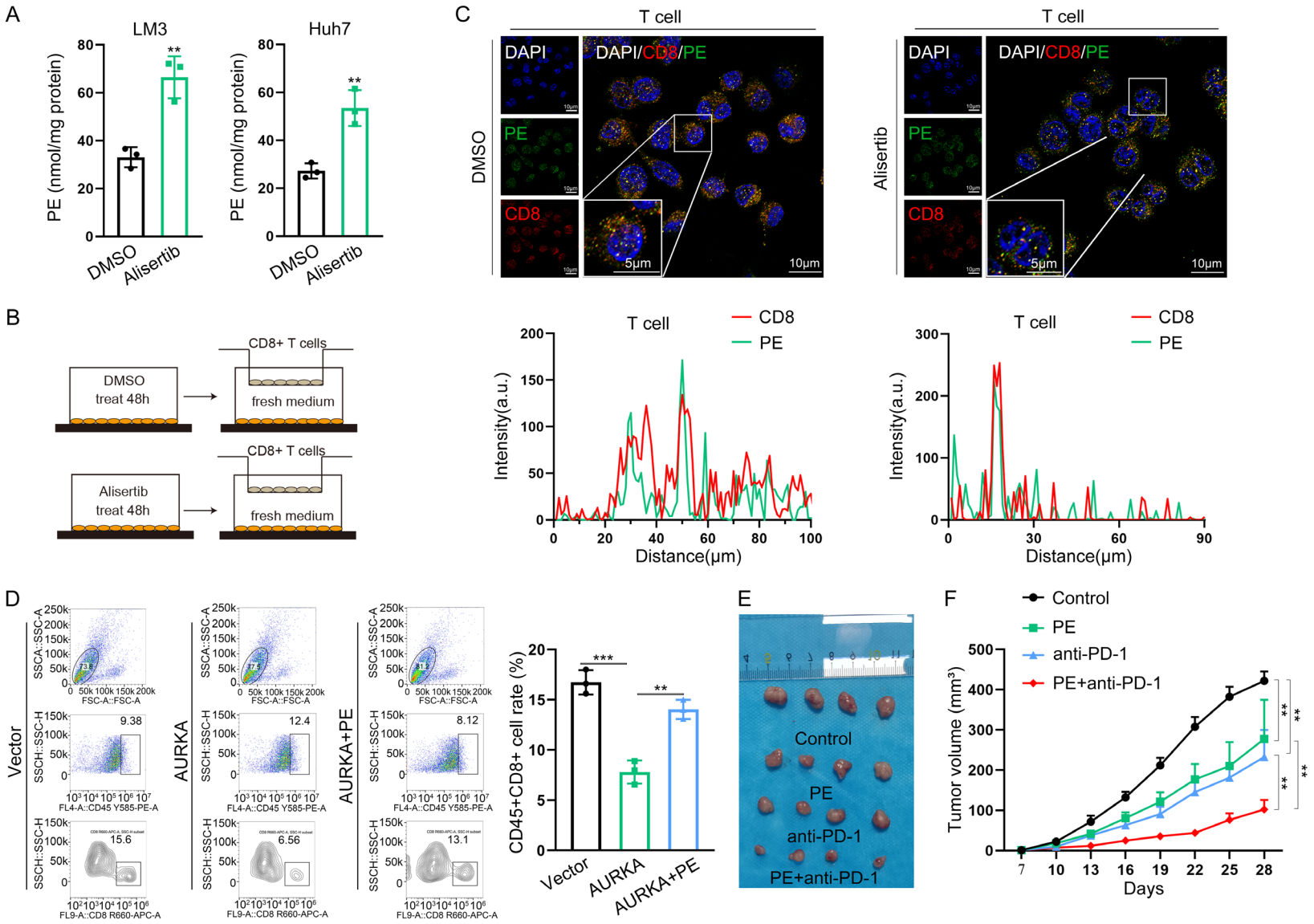
A
LM3
Huh7
PE (nmol/mg protein)
DMSO
Alisertib
B
CD8+ T cells
DMSO treat 48h
fresh medium
Alisertib treat 48h
C
T cell
DAPI
DAPI/CD8/PE
PE
CD8
DMSO
Alisertib
5μm
10μm
Intensity(a.u.)
Distance(μm)
D
Vector
AURKA
AURKA+PE
CD45+CD8+ cell rate (%)
E
Control
PE
anti-PD-1
PE+anti-PD-1
F
Tumor volume (mm³)
Days

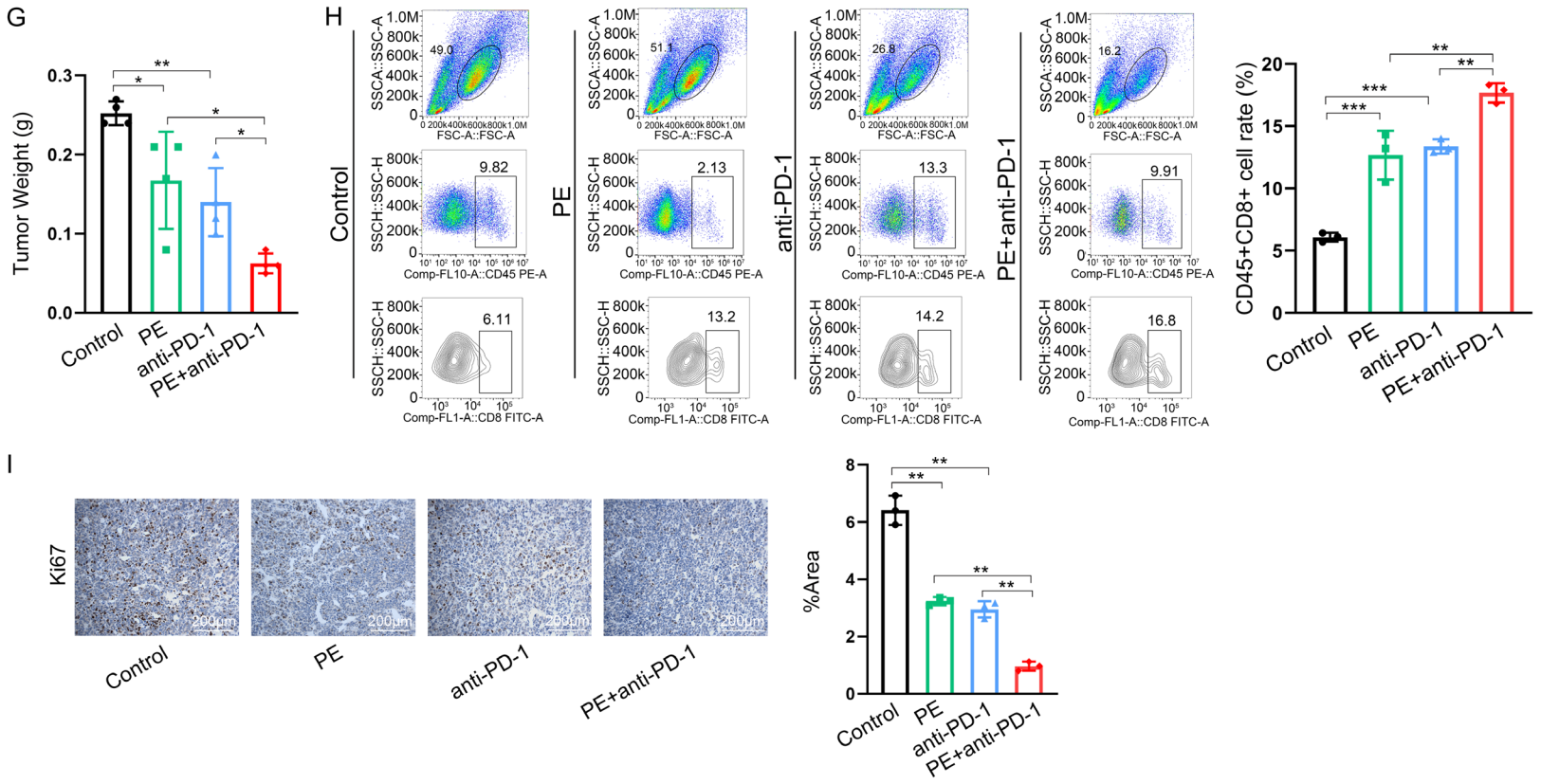

Figure 4. Aurora-A affects T cell infiltration and immune therapy efficacy in a PE-dependent manner. A. The impact of Alisertib on PE production in HCC cells was estimated. B. The co-culture model of $CD8^+$ T cells and LM3 cells treated with DMSO or Alisertib. C. The co-localization of PE and CD8 in T cells was observed by confocal fluorescence microscope. Scale bar = 5 or 10 μm. D. Changes in the accumulation of $CD45^+CD8^+$ T cells were assessed via flow cytometry. E. Images of tumors isolated from indicated groups of mice. F, G. Tumor growth curves and tumor weights were presented. H. Changes in the infiltration of $CD45^+CD8^+$ T cells in xenograft tumors were analyzed by flow cytometry. I. IHC analysis of Ki67 positive expression in xenograft tumors. Scale bar = 200 μm. $^*P < 0.05$, $^{**}P < 0.01$.

Alisertib-treated HCC cells absorbed more PE compared to those co-cultured with control HCC cells (**Figure 4C**). Moreover, the accumulation of $CD8^+$ T cells was suppressed by overexpression of AURKA, while this phenomenon was reversed upon further addition of PE (**Figure 4D**). These results suggest that Aurora-A inhibitor activates T cells by enhancing PE in HCC cells. Thereafter, we analyzed the PE-induced changes in HCC tumors that received immune therapy like anti-PD-1 treatment. It showed that the addition of PE or anti-PD-1 led to tumor inhibition, while the combination therapy induced much more suppression of tumor growth (**Figure 4E-G**). In contrast, $CD45^+CD8^+$ T cell rate in xenograft tumors was partially increased by either PE or anti-PD-1 therapy, but remarkably enhanced after combined treatment of PE and anti-PD-1 (**Figure 4H**). Also, the positive expression of Ki67 was reduced by PE or anti-PD-1 addition and further decreased after the tumors were processed simultaneously by PE and anti-PD-1 (**Figure 4I**). Based on these data, we summarized that upregulation of PE enhances the therapeutic effect of anti-PD-1 therapy on HCC downregulated upon AURKA overexpression. These data reveals that inhibiting Aurora-A induces PE production to promote T cell activation in HCC.

Aurora-A facilitates Drp1-Ser616 phosphorylation to hinder MAMs formation, disrupt PS/PE metabolism and impede ferroptosis

Previously, we discovered that Aurora-A disrupts PS/PE metabolism while having no significant effect on mitochondrial PSD, indicating Aurora-A might affect PS transport to affect PE synthesis. Thus, we explored how Aurora-A regulated PS at MAMs, the primary site of PS localization prior to mitochondrial import. The data of confocal fluorescence microscopy manifested that overexpression of AURKA hindered the co-localization of mitochondria with ER in HCC cells (**Figure 5A**). Drp1 is a pivotal protein involved in mitochondrial fission, and its activated status has recently proposed to participate in MAMs formation [21]. Hence, we detected the role of Aurora-A in regulating Drp1. Results indicated that AURKA overexpression had no effects on the levels of total Drp1 and Drp1 phosphorylated at Ser637 (named as Drp1-Ser637), but induced an obvious increase in the level of Drp1 phosphorylated at Ser616 (named Drp1-Ser616) (**Figure 5B**). In addition, more activated Drp1 (namely Drp1-Ser616) proteins were found to localize at mitochondria in HCC cells under AURKA overexpression (**Figure 5C**), indicating AURKA accelerated mitochondrial fission in HCC cells. Then, Drp1 inhibitor Mdivi-1 was applied to verify whether Aurora-A could affect MAMs formation, PE synthesis, and ferroptosis in a Drp1-dependent manner. As a result, the co-localization of mitochondria with ER suppressed by AURKA overexpression was reversed by Mdivi-1 (**Figure 5D**). Moreover, the repressive effects of AURKA overexpression on PE production, ROS, and MDA content were all counteracted by Mdivi-1-mediated Drp1 inhibition (**Figure 5E-G**). Similarly, AURKA overexpression-induced downregulation of ferroptosis-related genes at both mRNA and protein levels was also reversed by Mdivi-1 treatment (**Figure 5H**, **5I**). Therefore, we confirm that Aurora-A activates Drp1 to impede MAMs formation, PE production, and ferroptosis.

Aurora-A inhibitors contribute to MAMs formation and ferroptosis via inactivating Drp1

Finally, we tested whether Aurora-A inhibitor Alisertib exerted functions by affecting Drp1-Ser616 phosphorylation. We found that the level of Drp1-Ser616 was decreased by Alisertib (**Figure 6A**). Moreover, Alisertib-induced Aurora-A inhibition could promote the co-localization of ER and mitochondria, while this trend was reversed by additional Mdivi-1 treatment (**Figure 6B**). We then evaluated whether Aurora-A inhibitor affect MAMs formation, PE metabolism, and ferroptosis in a Drp1-dependent manner. Results showed that the co-localization of Drp1-Ser616 with mitochondria was lessened by Alisertib, while the reduced tendency was recovered after treatment with the Drp1 inhibitor Mdivi-1 (**Figure 6C**). In addition, Alisertib-caused enhancement on PE production was inversed after Mdivi-1 co-addition (**Figure 6D**). The stimulating effects of Alisertib on ROS, MDA, and the expression of ferroptosis-related genes were all counteracted after Mdivii-1-induced Drp1 inhibition (**Figure 6E-H**). To conclude, Aurora-A inhibitors accelerate MAMs formation, PE synthesis, and ferroptosis through activating Drp1.

Discussion

HCC ranks the third highest mortality rate among all tumor types worldwide. Recently, the

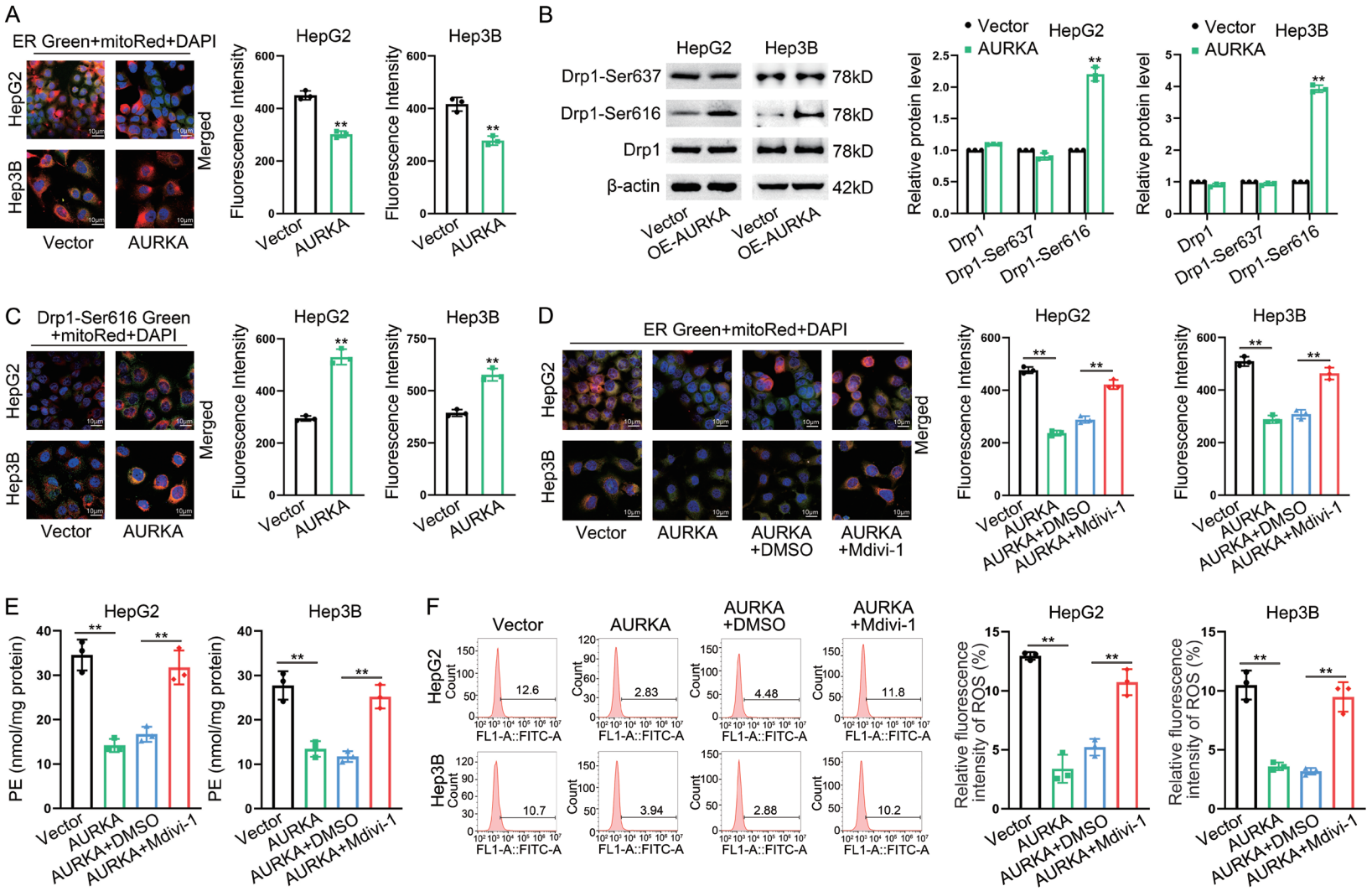
A
ER Green+mitoRed+DAPI
HepG2
Hep3B
Merged
Vector
AURKA
HepG2
Hep3B
Fluorescence Intensity
B
HepG2
Hep3B
Drp1-Ser637
Drp1-Ser616
Drp1
β-actin
78kD
42kD
Vector
OE-AURKA
Relative protein level
Drp1
Drp1-Ser637
Drp1-Ser616
C
Drp1-Ser616 Green
+mitoRed+DAPI
D
ER Green+mitoRed+DAPI
AURKA
+DMSO
AURKA
+Mdivi-1
E
PE (nmol/mg protein)
F
FL1-A::FITC-A
Count
12.6
2.83
4.48
11.8
10.7
3.94
2.88
10.2
Relative fluorescence intensity of ROS (%)

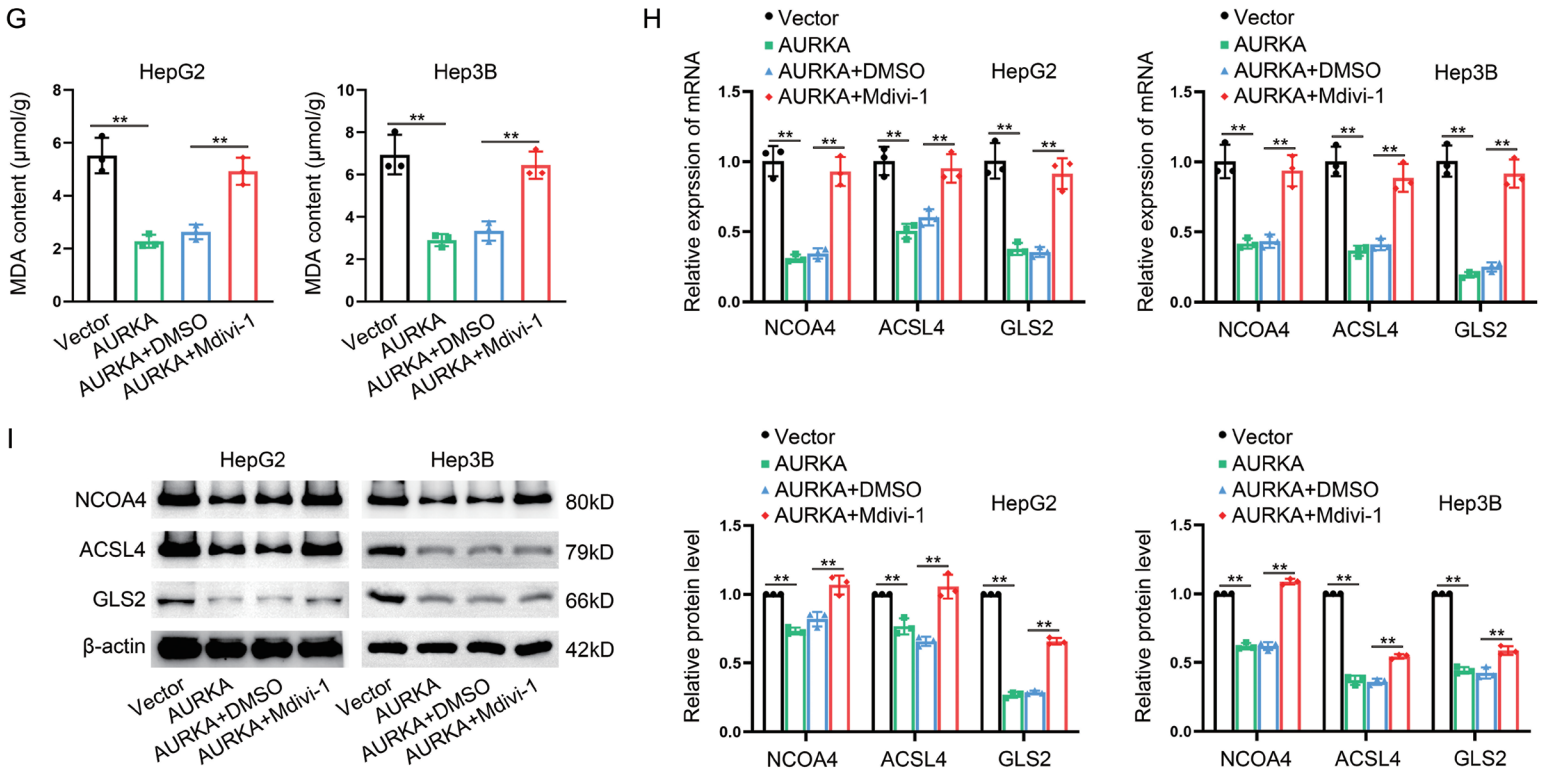

Figure 5. Aurora-A facilitates Drp1-Ser616 phosphorylation to hinder MAMs formation, PE synthesis and ferroptosis. A. Confocal images of ER and mitochondria in HCC cells under AURKA overexpression. Scale bar = 10 μm. B. Western blotting tested the impact of AURKA upregulation on the protein levels of total Drp1, Drp1-Ser637 and Drp1-Ser616 in HCC cells. C. Confocal images of the co-localization of Drp1 and mitochondria in indicated HCC cells. Scale bar = 10 μm. D. Confocal images of ER and mitochondria in HCC cells in response to different treatments. Scale bar = 10 μm. E. PE contents under different conditions were assessed. F. ROS levels in indicated HCC cells were evaluated via flow cytometry. G. MDA contents under different conditions were assessed. H, I. The alterations in the expressions of NCOA4, ACSL4 and GLS2 in indicated HCC cells were measured using RT-qPCR and western blotting. $^{**}P < 0.01$.

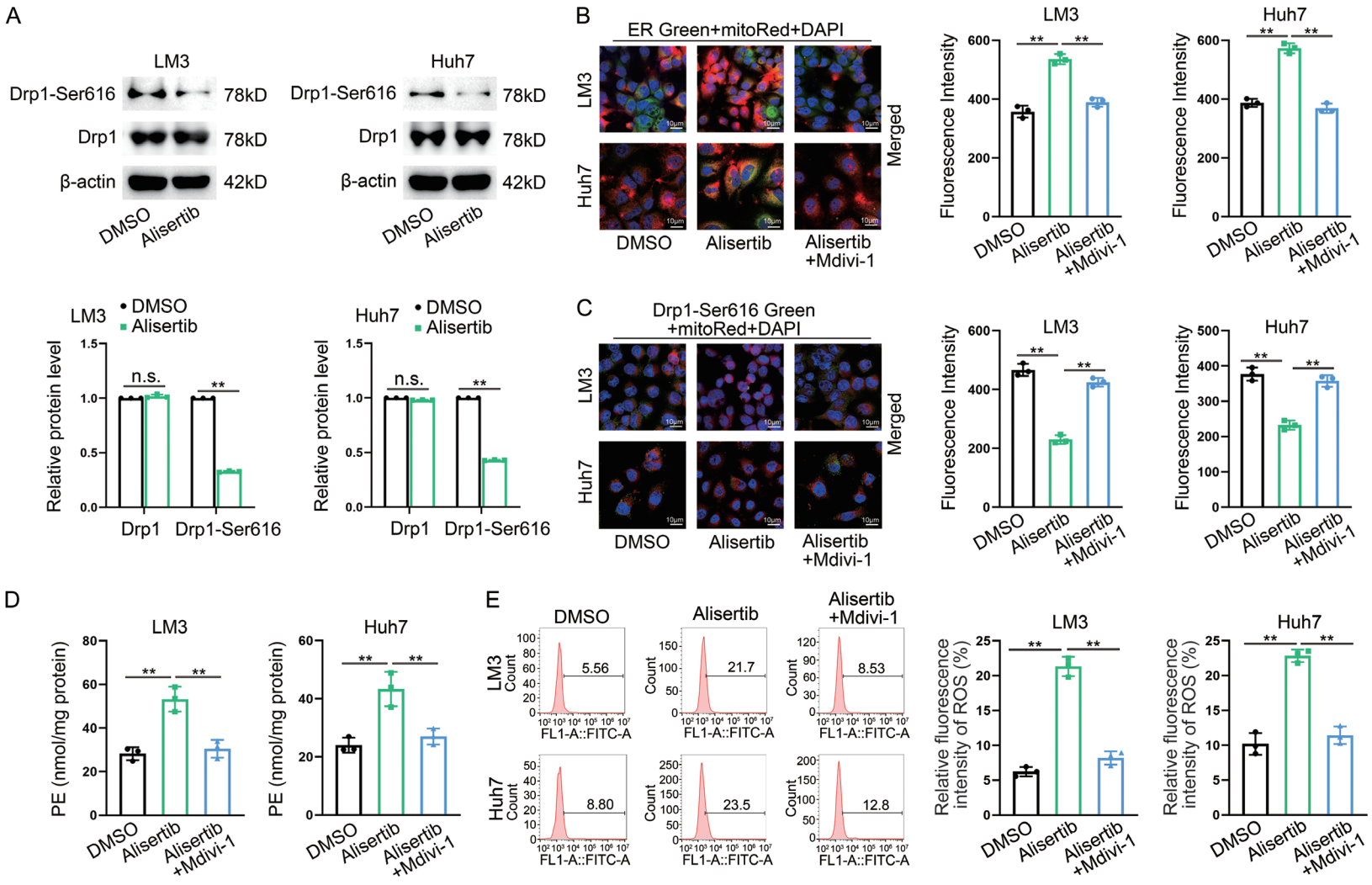
A
LM3
Drp1-Ser616
78kD
Drp1
78kD
β-actin
42kD
DMSO
Alisertib
Huh7
Drp1-Ser616
78kD
Drp1
78kD
β-actin
42kD
DMSO
Alisertib
LM3
DMSO
Alisertib
Relative protein level
n.s.
**
Drp1
Drp1-Ser616
Huh7
DMSO
Alisertib
Relative protein level
n.s.
**
Drp1
Drp1-Ser616
B
ER Green+mitoRed+DAPI
LM3
Huh7
Merged
DMSO
Alisertib
Alisertib +Mdivi-1
LM3
Fluorescence Intensity
**
**
DMSO
Alisertib
Alisertib +Mdivi-1
Huh7
Fluorescence Intensity
**
**
DMSO
Alisertib
Alisertib +Mdivi-1
C
Drp1-Ser616 Green +mitoRed+DAPI
LM3
Huh7
Merged
DMSO
Alisertib
Alisertib +Mdivi-1
LM3
Fluorescence Intensity
**
**
DMSO
Alisertib
Alisertib +Mdivi-1
Huh7
Fluorescence Intensity
**
**
DMSO
Alisertib
Alisertib +Mdivi-1
D
LM3
PE (nmol/mg protein)
**
**
DMSO
Alisertib
Alisertib +Mdivi-1
Huh7
PE (nmol/mg protein)
**
**
DMSO
Alisertib
Alisertib +Mdivi-1
E
DMSO
Alisertib
Alisertib +Mdivi-1
LM3
Count
5.56
21.7
8.53
FL1-A::FITC-A
Huh7
Count
8.80
23.5
12.8
FL1-A::FITC-A
LM3
Relative fluorescence intensity of ROS (%)
**
**
DMSO
Alisertib
Alisertib +Mdivi-1
Huh7
Relative fluorescence intensity of ROS (%)
**
**
DMSO
Alisertib
Alisertib +Mdivi-1

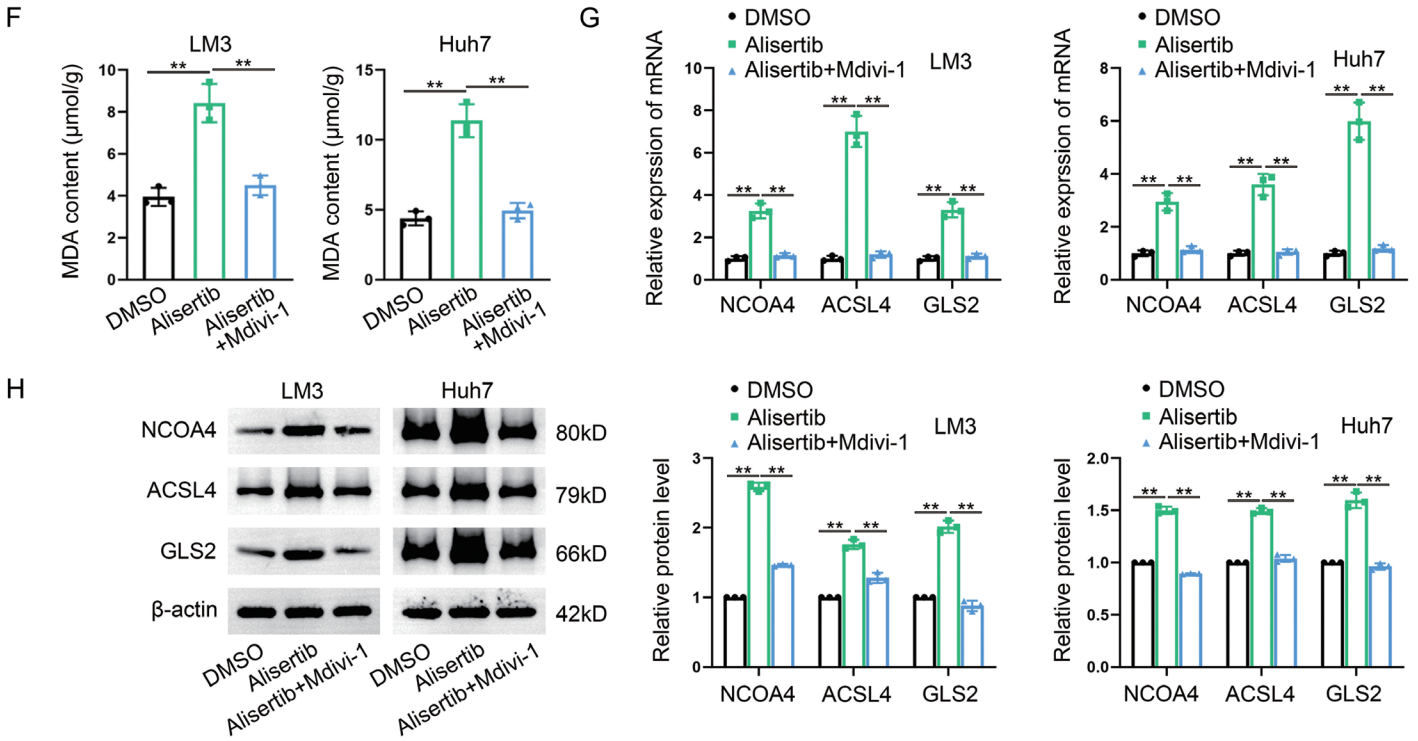

Figure 6. Aurora-A inhibitors affect MAMs formation, PE synthesis and ferroptosis via Drp1. A. The effects of Alisertib on the levels of Drp1-Ser616 in HCC cells were evaluated by western blotting. B. Confocal images of ER and mitochondria in HCC cells treated with DMSO, Alisertib or Alisertib+Mdivi-1. Scale bar = 10 μm. C. Confocal images of Drp1 and mitochondria in HCC cells with different treatments. Scale bar = 10 μm. D-F. The changes in PE production, ROS and MDA content under different conditions were evaluated. G, H. The expressions of NCOA4, ACSL4 and GLS2 in indicated HCC cells were determined by RT-qPCR and western blotting. $^{**}P < 0.01$, n.s.: not significant.

FDA has approved two immune-checkpoint inhibitors (ICIs) targeting PD-1, namely pembrolizumab and nivolumab, as second-line treatments for advanced HCC [22]. However, only a small percentage of patients respond to immunotherapy, and most of them finally develop resistance [23]. Hence, searching for new biomarkers to alleviate the resistance is vital. Here, we focused on Aurora-A, a serine/threonine protein kinase that is overexpressed in HCC. Aurora-A has been proven to be overexpressed and highly related to poor prognosis in several malignancies including HCC [24, 25]. According to previous studies, Aurora-A and its inhibitors can modulate the radioresistance and chemoresistance of HCC cells [8, 11]. Presently, we demonstrated that Aurora-A inhibitor markedly enhanced the anti-tumor effect of anti-PD-1 therapy on HCC. The results indicated Aurora-A as a potential target for improving immunotherapy on HCC.

The occurrence of HCC is often accompanied by a large amount of metabolic reprogramming to create a suitable microenvironment for the growth and proliferation of cancer cells [26]. Through metabolomics analysis, we demonstrated that knockdown AURKA significantly augmented PE biosynthesis. As a phospholipid abundant in membranes, PE plays pivotal parts in multifarious membrane functions [27]. A previous report unveiled lower PE concentrations in HCC patients than in controls [28]. Furthermore, PE is reported to participate in regulating autophagy [29], and changes in its synthesis can affect cancer cell proliferation [16]. Significantly, PE biosynthesis is proposed as a new target for cancer chemotherapy [30]. Besides, PE has high relevance to immune function [31-33]. In this study, we unveiled that inhibiting Aurora-A targeted PE biosynthesis to enhance the sensitivity of HCC cells and tumors to anti-PD-1.

Ferroptosis is a kind of necrosis that occurs in cellular membranes. Usually, it is an iron-dependent process resulting from lipid peroxidation and featured by the accumulation of lipid peroxides [34]. PE is one of phospholipids, which is responsible for lipid peroxidation-induced ferroptosis [18]. Additionally, direct PE oxygenation is a ferroptosis signal [35]. Here, we uncovered that Aurora-A hampered ferroptosis by inhibiting PE production. Meanwhile, targeting ferroptosis is also suggested as a potential pathway for cancer therapy [36, 37], including immunotherapy [38]. These reports further support our findings that targeting Aurora-A strengthened the efficacy of anti-PD-1 in HCC via facilitating PE biosynthesis and subsequent ferroptosis.

MAMs are dynamic membrane coupling regions formed by the connection of the mitochondrial outer membrane and ER [39]. Generally, PS is transported from ER to mitochondria via MAMs and then transformed to PE via PSD-mediated decarboxylation in mitochondria [40]. The current study verified that Aurora-A modulated PS/PE metabolism in HCC cells by suppressing MAMs formation. Aberrant MAMs formation induces various pathological events [41]. Drp1 is a main controller of mitochondrial fission through being phosphorylated at Ser616 and Ser637 [42, 43]. More importantly, excessive mitochondrial fission hinders MAMs formation [44]. In the present study, we found that Aurora-A facilitated Drp1 phosphorylation at Ser616, thus contributing to mitochondrial fission and reducing MAMs formation.

In conclusion, our findings indicated that Aurora-A impeded PE synthesis to improve anti-PD-1 efficacy by facilitating Drp1-Ser616 phosphorylation to disrupt MAM formation and suppress ferroptosis. The results hint that Aurora-A inhibitors might be suitable for combination with immune therapy in HCC. However, the current study has some limitations. Our experimental results showed that AURKA knockdown led to an overall increase in cellular PS levels, suggesting that AURKA might act as an upstream regulator of PS. Therefore, our findings indicated that AURKA likely influences PS/PE metabolism through two distinct pathways. On one hand, it may exert acute effect by regulating PS transport from the ER to mitochondria; on the other hand, it may exert chronical effect through modulating PS synthesis/degradation. The precise upstream regulatory mechanisms of AURKA on PS will be a key focus for our future research.

Acknowledgements

This study was supported by the Natural Science Foundation of Jiangsu Province Academy of Traditional Chinese Medicine (2024-YZRKXJJ20); National Natural Science Foundation of China (No. 82073164); Natural Science

Foundation of Chongqing, China (CSTB2024-NSCQ-MSX0914); and Qijiang District Science and Technology Plan Project (No. 2024082).

Disclosure of conflict of interest

None.

Abbreviations

Aurora-A, Aurora Kinase A Protein; HCC, Hepatocellular carcinoma; PE, phosphatidylethanolamine; PSD, phosphatidylserine decarboxylase; Drp1, dynein-related protein; MAM, mitochondrial-associated membrane; PS, phosphatidylserine; PD-1, Programmed cell death protein 1; THLE2, The healthy liver-derived human cell line; ESI, electrospray ionization; SDS-PAGE, sodium dodecyl sulfate-polyacrylamide gel electrophoresis; NC, nitrocellulose; IHC, Immunohistochemistry.

Address correspondence to: Dr. Shiyun Cui, Department of Oncology, The First Affiliated Hospital of Nanjing Medical University, 300 Guangzhou Road, Nanjing 210029, Jiangsu, P. R. China. Tel: +86-13805195043; E-mail: cuishiyun@njmu.edu.cn; Dr. Changchun Sun, Department of Oncology, Jingjiang People's Hospital Affiliated to Yangzhou University, 28 Zhongzhou Road, Jingjiang 214504, Jiangsu, P. R. China. Tel: +86-18862807813; E-mail: sunchangchun11@163.com

References

[1] Sung H, Ferlay J, Siegel RL, Laversanne M, Soerjomataram I, Jemal A and Bray F. Global Cancer Statistics 2020: GLOBOCAN estimates of incidence and mortality worldwide for 36 cancers in 185 countries. CA Cancer J Clin 2021; 71: 209-249.

[2] Sidali S, Trépo E, Sutter O and Nault JC. New concepts in the treatment of hepatocellular carcinoma. United European Gastroenterol J 2022; 10: 765-774.

[3] Li Q, Han J, Yang Y and Chen Y. PD-1/PD-L1 checkpoint inhibitors in advanced hepatocellular carcinoma immunotherapy. Front Immunol 2022; 13: 1070961.

[4] Correction to Lancet Oncol 2018; 19: 940-52. Lancet Oncol 2018; 19: e440.

[5] Bolanos-Garcia VM. Aurora kinases. Int J Biochem Cell Biol 2005; 37: 1572-1577.

[6] Wang R, Wang JH, Chu XY, Geng HC and Chen LB. Expression of STK15 mRNA in hepatocellular carcinoma and its prognostic significance. Clin Biochem 2009; 42: 641-647.

[7] Lee SY, Lee GR, Woo DH, Park NH, Cha HJ, Moon YH and Han IS. Depletion of Aurora A leads to upregulation of FoxO1 to induce cell cycle arrest in hepatocellular carcinoma cells. Cell Cycle 2013; 12: 67-75.

[8] Shen ZT, Chen Y, Huang GC, Zhu XX, Wang R and Chen LB. Aurora-a confers radioresistance in human hepatocellular carcinoma by activating NF-κB signaling pathway. BMC Cancer 2019; 19: 1075.

[9] Zhang K, Chen J, Chen D, Huang J, Feng B, Han S, Chen Y, Song H, De W, Zhu Z, Wang R and Chen L. Aurora-A promotes chemoresistance in hepatocelluar carcinoma by targeting NF-kappaB/microRNA-21/PTEN signaling pathway. Oncotarget 2014; 5: 12916-12935.

[10] Zhu Q, Yu X, Zhou ZW, Zhou C, Chen XW and Zhou SF. Inhibition of Aurora A kinase by Alisertib induces autophagy and cell cycle arrest and increases chemosensitivity in human hepatocellular carcinoma HepG2 cells. Curr Cancer Drug Targets 2017; 17: 386-401.

[11] Zhang K, Wang T, Zhou H, Feng B, Chen Y, Zhi Y and Wang R. A Novel Aurora-A Inhibitor (MLN8237) synergistically enhances the antitumor activity of sorafenib in hepatocellular carcinoma. Mol Ther Nucleic Acids 2018; 13: 176-188.

[12] Faubert B, Solmonson A and DeBerardinis RJ. Metabolic reprogramming and cancer progression. Science 2020; 368: eaaw5473.

[13] Xia L, Oyang L, Lin J, Tan S, Han Y, Wu N, Yi P, Tang L, Pan Q, Rao S, Liang J, Tang Y, Su M, Luo X, Yang Y, Shi Y, Wang H, Zhou Y and Liao Q. The cancer metabolic reprogramming and immune response. Mol Cancer 2021; 20: 28.

[14] Cheng A, Zhang P, Wang B, Yang D, Duan X, Jiang Y, Xu T, Jiang Y, Shi J, Ding C, Wu G, Sang Z, Wu Q, Wang H, Wu M, Zhang Z, Pan X, Pan YY, Gao P, Zhang H, Zhou CZ, Guo J and Yang Z. Aurora-A mediated phosphorylation of LDHB promotes glycolysis and tumor progression by relieving the substrate-inhibition effect. Nat Commun 2019; 10: 5566.

[15] Miao YZ, Wang J, Hao SY, Deng YX, Zhang Z, Jin ZP, Liu DY, Zhang SD, Wan H, Ji N and Feng J. The inhibition of Aurora A kinase regulates phospholipid remodeling by upregulating LPCAT1 in glioblastoma. Neoplasma 2023; 70: 260-271.

[16] Pandey SK, Paul A, Shteinfer-Kuzmine A, Zalk R, Bunz U and Shoshan-Barmatz V. SMAC/Diablo controls proliferation of cancer cells by regulating phosphatidylethanolamine synthesis. Mol Oncol 2021; 15: 3037-3061.

[17] Chang Y, Wang C, Zhu J, Zheng S, Sun S, Wu Y, Jiang X, Li L, Ma R and Li G. SIRT3 ameliorates diabetes-associated cognitive dysfunction via regulating mitochondria-associated ER membranes. J Transl Med 2023; 21: 494.

[18] Lee JY, Kim WK, Bae KH, Lee SC and Lee EW. Lipid metabolism and ferroptosis. Biology (Basel) 2021; 10: 184.
[19] Hsu SK, Li CY, Lin IL, Syue WJ, Chen YF, Cheng KC, Teng YN, Lin YH, Yen CH and Chiu CC. Inflammation-related pyroptosis, a novel programmed cell death pathway, and its crosstalk with immune therapy in cancer treatment. Theranostics 2021; 11: 8813-8835.
[20] Chen H, Hu J, Xiong X, Chen H, Lin B, Chen Y, Li Y, Cheng D and Li Z. AURKA inhibition induces Ewing's sarcoma apoptosis and ferroptosis through NPM1/YAP1 axis. Cell Death Dis 2024; 15: 99.
[21] Duan C, Liu R, Kuang L, Zhang Z, Hou D, Zheng D, Xiang X, Huang H, Liu L and Li T. Activated Drp1 initiates the formation of endoplasmic reticulum-mitochondrial contacts via Shrm4-mediated actin bundling. Adv Sci (Weinh) 2023; 10: e2304885.
[22] Donne R and Lujambio A. The liver cancer immune microenvironment: therapeutic implications for hepatocellular carcinoma. Hepatology 2023; 77: 1773-1796.
[23] Wang Z, Wang Y, Gao P and Ding J. Immune checkpoint inhibitor resistance in hepatocellular carcinoma. Cancer Lett 2023; 555: 216038.
[24] Yan M, Wang C, He B, Yang M, Tong M, Long Z, Liu B, Peng F, Xu L, Zhang Y, Liang D, Lei H, Subrata S, Kelley KW, Lam EW, Jin B and Liu Q. Aurora-A kinase: a potent oncogene and target for cancer therapy. Med Res Rev 2016; 36: 1036-1079.
[25] Jeng YM, Peng SY, Lin CY and Hsu HC. Overexpression and amplification of Aurora-A in hepatocellular carcinoma. Clin Cancer Res 2004; 10: 2065-2071.
[26] Wang Q, Tan Y, Jiang T, Wang X, Li Q, Li Y, Dong L, Liu X and Xu G. Metabolic reprogramming and its relationship to survival in hepatocellular carcinoma. Cells 2022; 11: 1066.
[27] Watanabe Y, Watanabe Y and Watanabe S. Structural basis for phosphatidylethanolamine biosynthesis by bacterial phosphatidylserine decarboxylase. Structure 2020; 28: 799-809. e795.
[28] Cotte AK, Cottet V, Aires V, Mouillot T, Rizk M, Vinault S, Binquet C, de Barros JP, Hillon P and Delmas D. Phospholipid profiles and hepatocellular carcinoma risk and prognosis in cirrhotic patients. Oncotarget 2019; 10: 2161-2172.
[29] Rockenfeller P, Koska M, Pietrocola F, Minois N, Knittelfelder O, Sica V, Franz J, Carmona-Gutierrez D, Kroemer G and Madeo F. Phosphatidylethanolamine positively regulates autophagy and longevity. Cell Death Differ 2015; 22: 499-508.
[30] Guan Y, Chen X, Wu M, Zhu W, Arslan A, Takeda S, Nguyen MH, Majeti R, Thomas D, Zheng M and Peltz G. The phosphatidylethanolamine biosynthesis pathway provides a new target for cancer chemotherapy. J Hepatol 2020; 72: 746-760.
[31] Zenarruzabeitia O, Vitallé J, Eguizabal C, Simhadri VR and Borrego F. The biology and disease relevance of cd300a, an inhibitory receptor for phosphatidylserine and phosphatidylethanolamine. J Immunol 2015; 194: 5053-5060.
[32] Bae M, Cassilly CD, Liu X, Park SM, Tusi BK, Chen X, Kwon J, Filipčík P, Bolze AS, Liu Z, Vlamakis H, Graham DB, Buhrlage SJ, Xavier RJ and Clardy J. Akkermansia muciniphila phospholipid induces homeostatic immune responses. Nature 2022; 608: 168-173.
[33] Uehara T, Fujiwara T, Takeda K, Kunisada T, Ozaki T and Udono H. Immunotherapy for bone and soft tissue sarcomas. Biomed Res Int 2015; 2015: 820813.
[34] Dixon SJ, Lemberg KM, Lamprecht MR, Skouta R, Zaitsev EM, Gleason CE, Patel DN, Bauer AJ, Cantley AM, Yang WS, Morrison B 3rd and Stockwell BR. Ferroptosis: an iron-dependent form of nonapoptotic cell death. Cell 2012; 149: 1060-1072.
[35] Kagan VE, Mao G, Qu F, Angeli JP, Doll S, Croix CS, Dar HH, Liu B, Tyurin VA, Ritov VB, Kapralov AA, Amoscato AA, Jiang J, Anthonymuthu T, Mohammadyani D, Yang Q, Proneth B, Klein-Seetharaman J, Watkins S, Bahar I, Greenberger J, Mallampalli RK, Stockwell BR, Tyurina YY, Conrad M and Bayır H. Oxidized arachidonic and adrenic PEs navigate cells to ferroptosis. Nat Chem Biol 2017; 13: 81-90.
[36] Tong X, Tang R, Xiao M, Xu J, Wang W, Zhang B, Liu J, Yu X and Shi S. Targeting cell death pathways for cancer therapy: recent developments in necroptosis, pyroptosis, ferroptosis, and cuproptosis research. J Hematol Oncol 2022; 15: 174.
[37] Lei G, Zhuang L and Gan B. Targeting ferroptosis as a vulnerability in cancer. Nat Rev Cancer 2022; 22: 381-396.
[38] Xu H, Ye D, Ren M, Zhang H and Bi F. Ferroptosis in the tumor microenvironment: perspectives for immunotherapy. Trends Mol Med 2021; 27: 856-867.
[39] Mao H, Chen W, Chen L and Li L. Potential role of mitochondria-associated endoplasmic reticulum membrane proteins in diseases. Biochem Pharmacol 2022; 199: 115011.
[40] Vance JE. Phospholipid synthesis and transport in mammalian cells. Traffic 2015; 16: 1-18.
[41] Barazzuol L, Giamogante F and Calì T. Mitochondria Associated Membranes (MAMs): ar-

chitecture and physiopathological role. Cell Calcium 2021; 94: 102343.
[42] Schmitt K, Grimm A, Dallmann R, Oettinghaus B, Restelli LM, Witzig M, Ishihara N, Mihara K, Ripperger JA, Albrecht U, Frank S, Brown SA and Eckert A. Circadian control of DRP1 activity regulates mitochondrial dynamics and bioenergetics. Cell Metab 2018; 27: 657-666. e655.
[43] Ramalingam M, Jang S, Hwang J, Kim B, Cho HH, Kim E and Jeong HS. Neuroprotective effects of the neural-induced adipose-derived stem cell secretome against rotenone-induced mitochondrial and endoplasmic reticulum dysfunction. Int J Mol Sci 2023; 24: 5622.
[44] Cherubini M, Lopez-Molina L and Gines S. Mitochondrial fission in Huntington's disease mouse striatum disrupts ER-mitochondria contacts leading to disturbances in Ca(2+) efflux and Reactive Oxygen Species (ROS) homeostasis. Neurobiol Dis 2020; 136: 104741.

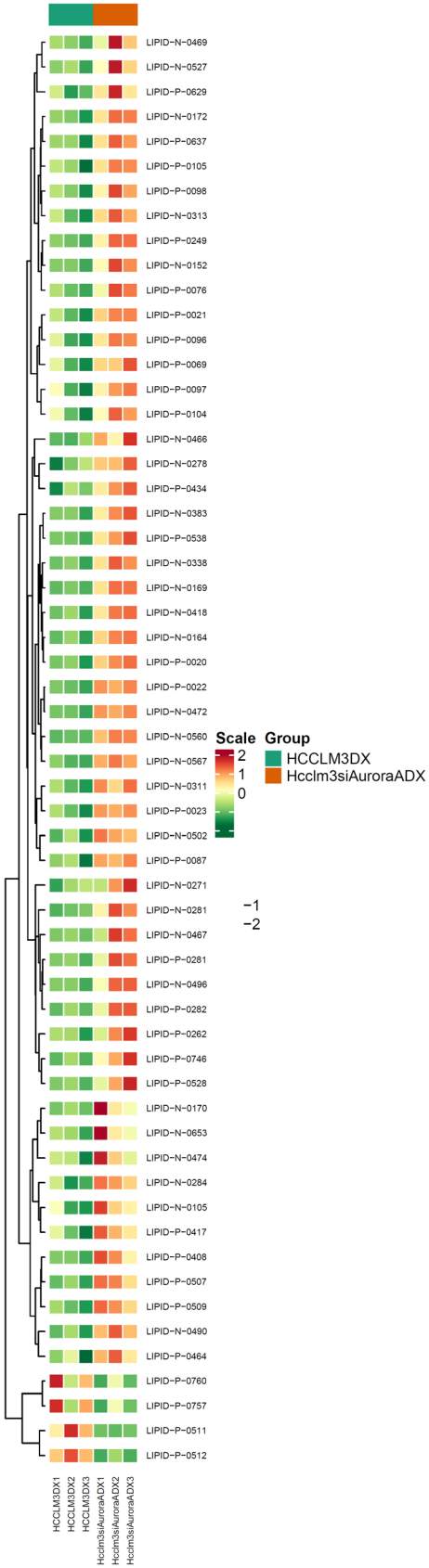

Figure S1. Non-targeted metabolomics analysis of metabolites influenced by AURKA knockdown.

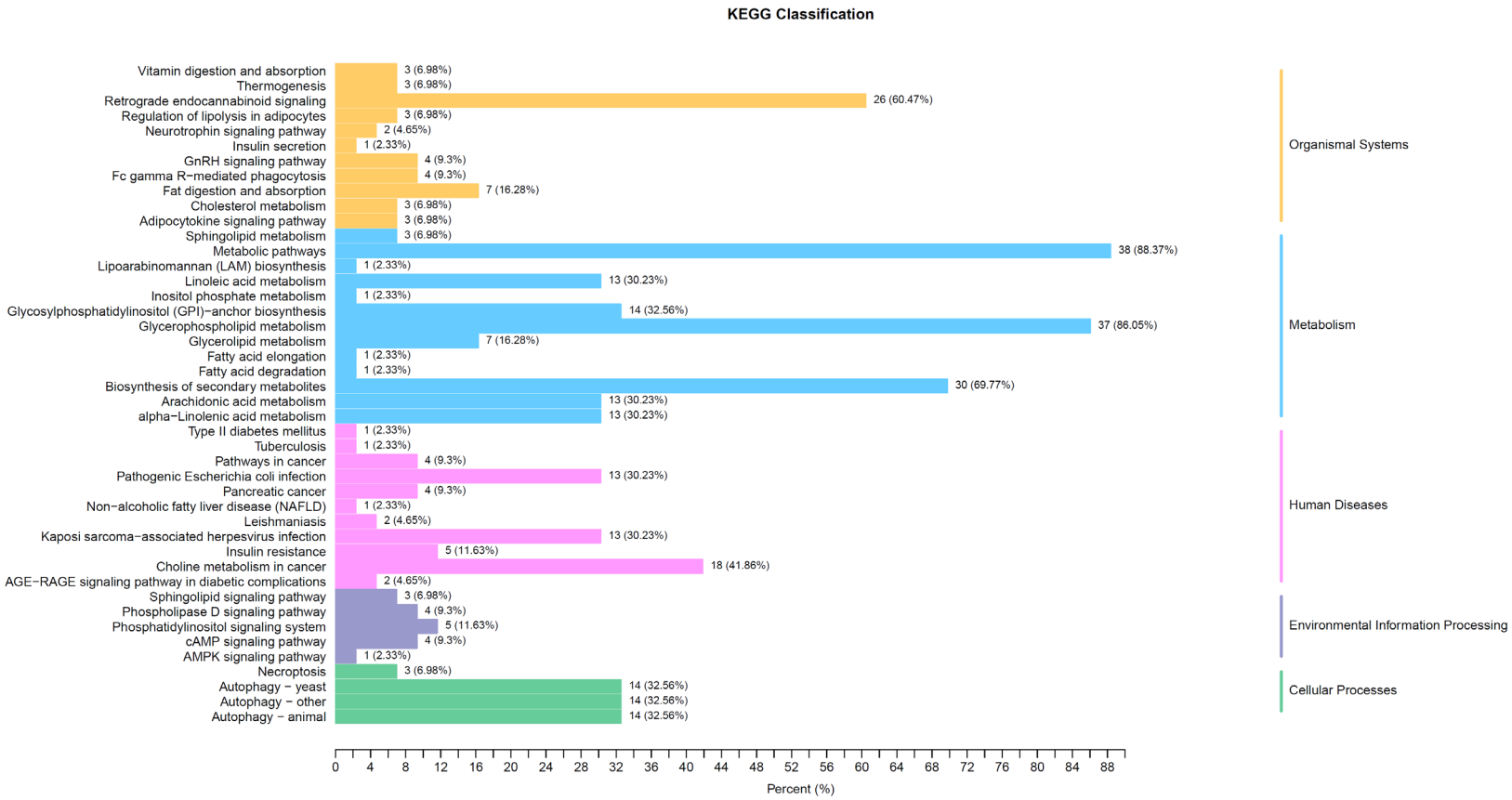

Figure S2. GO analyses of metabolites significantly regulated by AURKA.

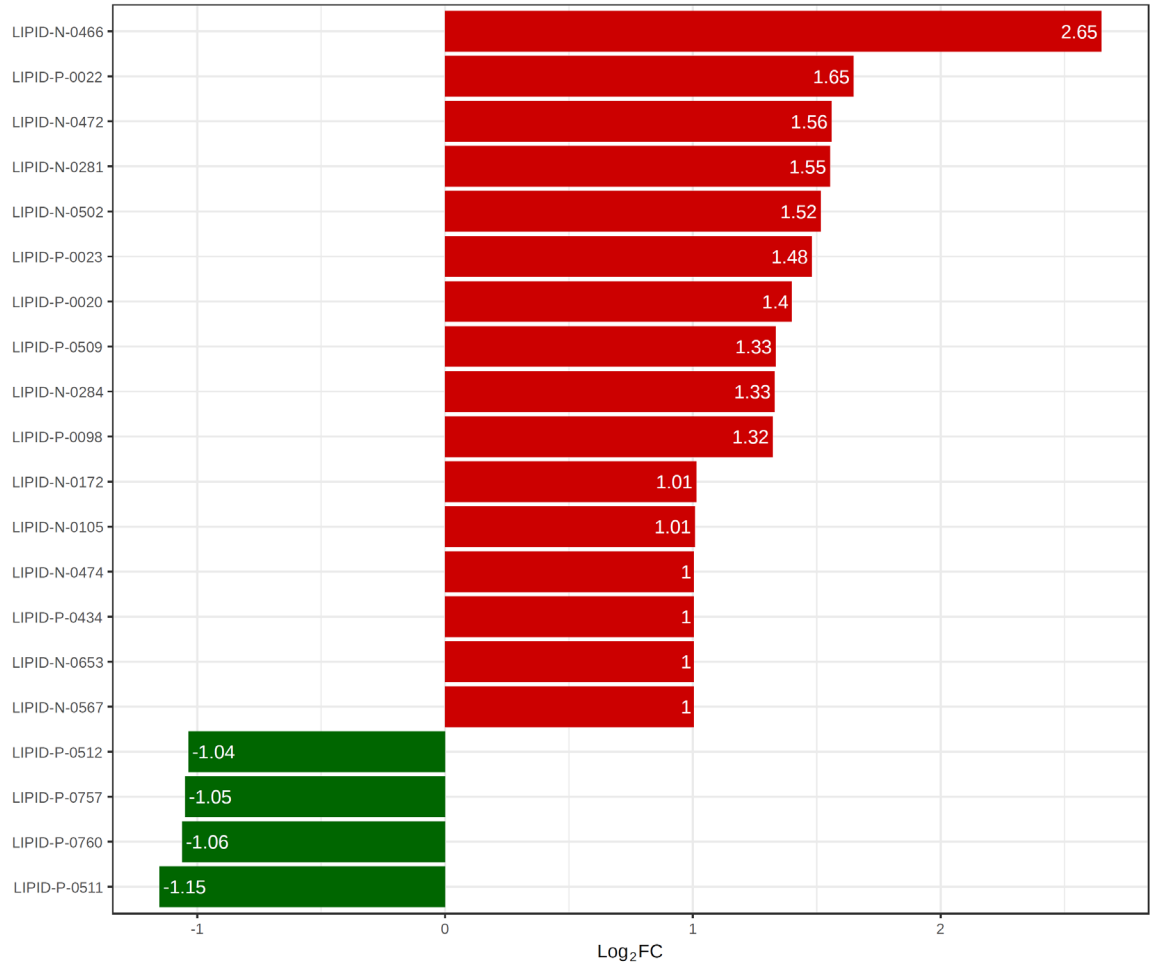

Figure S3. KEGG analyses of metabolites significantly regulated by AURKA.